The Thermodynamic Analysis of the Swirl Flow Applied to Micro-Heat Sink

Dorin Lelea*

University "Politehnica" of Timisoara, Faculty of Mechanical Engineering, B-dul Mihai Viteazu nr. 1, 300222 Timisoara, Romania

Abstract: This paper deals with the numerical analysis of a microtube heat sink with tangential impingement jet feeding. The inlet channel covers only a quarter of the tube perimeter so the swirl flow is settled in the tubes. It is expected that heat transfer between the liquid flow and silicon substrate will be improved. The paper also sets up a discussion about the thermodynamic and hydrodynamic aspect of the swirl flow and the benefits resulting from this behavior. The water with the constant physical properties is used as the working fluid and laminar flow regime is considered. Comparison between the classic microtube heat sink with frontal feeding and a microtube heat sink used in this research has also been done.

INTRODUCTION

The thermal management of the electronic and power sources became a challenging issue in the last decade because of both, miniaturization and an increase in the heat transfer rate. The various cooling solutions have been proposed that use both the single and two-phase heat transfer. Considering that this paper deals with a single phase heat transfer of the water, only these cooling schemes will be considered.

The advantage of the single-phase microchannel heat sink is based on an increase in the heat transfer coefficient as the hydraulic diameter is decreasing. Also, the channel walls are acting as the fins that increase the heat transfer area. In the case of the microchannel heat sinks, the investigations are made for the single layer [1-7] and double layer arrangements [8-10]. The research has been made experimentally and numerically although the analytical solution based on a porous model approach has been announced [11,12]. The various optimization techniques have been employed to improve the heat sink performances [13,14]. In addition, the review chapters on micro-heat sinks might be found in [15,16].

Contrary to the microchannel heat sinks, Soliman *et al.* [17] presented the numerical analysis of a microtube heat sink. The laminar heat transfer of the water through the microtubes is considered. It was found that proposed heat sink has higher thermal resistance and needs lower pumping power compared with a microchannel heat sink, for the same Re and hydraulic diameter. On the other hand, based on unit pumping power, the microtube heat sink can dissipate slightly larger heat rate than a microchannel heat sink.

Besides this, Ryu *et al*. [18] have presented the numerical analysis of a manifold microchannel heat sink. It is concluded that this heat sink has better performances than the classic microchannel heat sink, lower thermal resistance and more uniform temperature distribution for the same pumping power. To obtain the best heat transfer characteristics, an optimization of the heat sink geometric parameters is done.

For the microchannel heat sinks with large length to diameter ratio and uniform inlet velocity feeding of the channels, the fluid flow and thermal regime are fully developed for almost the total channel length. As the heat transfer coefficient is lower in this case, another option is to induce flow instabilities and to set up developing fluid flow and heat transfer along the channel.

Sung and Mudawar [19] analyzed the hybrid jet impingement microchannel heat sink in turbulent heat transfer and fluid flow. Observed vorticity effects have the large influence on a zone outside the impingement jet. The stronger attachment of the fluid flow to the heated surface for higher Re is observed. It was also proposed the improved design of the heat sink based on the analysis that lowers the temperature of the heated surface.

Bello-Ochende *et al.* [20, 21] presented the geometric optimization of a micro-channel heat sink. The results show the reduction in thermal resistance of about 8 %, when applied to a known micro-channel heat sink. It was also observed that degree of freedoms provided by the aspect ratio and the solid volume fraction, has a strong effect on the peak temperature and the maximum thermal conductance.

Following this survey of the cooling schemes used for the electronic and high power devices, the microtube heat sink with impingement jet is analyzed. In this case the fluid is attached to the heated surface. To extend this behavior, the inlet impingement jet is tangentially positioned to the microtube.

PROBLEM DESCRIPTION AND NUMERICAL DETAILS

The microtube heat sink assembly proposed for the numerical analysis is presented in the Fig. (**1**). It can be remarked that feeding of the microtube heat sink is realized through the gaps positioned on a top surface of the heat sink.

*Address correspondence to this author at the University "Politehnica" of Timisoara, Faculty of Mechanical Engineering , B-dul Mihai Viteazu nr. 1, 300222 Timisoara, Romania; Tel: +40 256403670; Fax: +40 256403669; E-mail: ldorin@mec.utt.ro

1874-396X/08

The cross section of the microtube with the inlet channel is presented in the Fig. (**2**). The microtube is thermally and hydrodynamically symmetrical with respect to the boundary positioned at a half-length of the microtube. So, only the left part of the microtube is analyzed. Lelea *et al.* [22] and Lelea [23] have analyzed numerically and experimentally the laminar heat transfer and fluid flow of the water through a single microtube and concluded that conventional theories are applicable to the microtubes with diameters down to 100 μm.

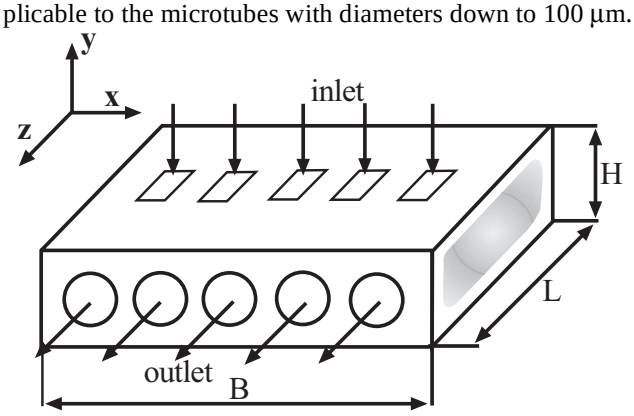

Fig. (1). The microtube heat sink assembly with tangential impingement jet.

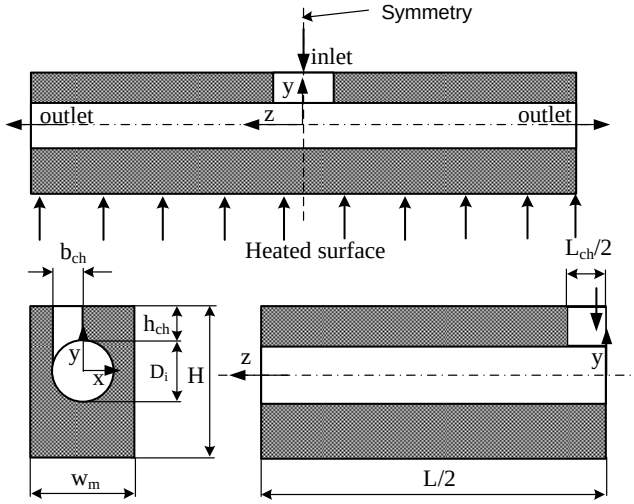

Fig. (2). The single microtube geometry.

Therefore the Navier-Stokes equations can be used to analyze the heat transfer and fluid flow through the micro-heat sink:

The conservation of mass

$$\frac{\partial(\rho \cdot u_i)}{\partial x_i} = 0 \tag{1}$$

The conservation of momentum

$$\frac{\partial(u_i \cdot \rho \cdot u_j)}{\partial x_i} = -\frac{\partial p}{\partial x_i} + \frac{\partial}{\partial x_i}\left(\mu \frac{\partial u_j}{\partial x_i}\right) \tag{2}$$

The conservation of energy

$$\frac{\partial(\rho \cdot c_p \cdot u_i \cdot T)}{\partial x_i} = \frac{\partial}{\partial x_i}\left(k \frac{\partial T}{\partial x_i}\right) \tag{3}$$

Table 1. The Geometry, Thermal and Flow Conditions of the Micro-Tube Heat Sink

B, cm	1	w_m, μm	350
H, μm	500	D_i, μm	300
L, cm	1	N	30
b_{ch}, μm	150	M, kg/s	$10\cdot10^{-5}$ -$110\cdot10^{-5}$
L_{ch}, mm	1	Re	212 - 2335
h_{ch}, μm	50	T_{in}, K	293

For the micro-tube heat sink presented in this paper, the following boundary conditions are settled:

The fluid flow is stationary, incompressible and laminar;

The fluid properties (density, thermal conductivity, viscosity and specific heat) are constant and evaluated for the inlet temperature, as follows: k_f = 0.6 W/m K, c_p = 4182 J/kg K, μ = 0.001 Pa s, ρ = 998.2 kg/m^3; for silicon k_s = 125.5 W/m K. The uniform heat flux is imposed on a bottom surface of the heat sink, q = 100 W/cm^2.

The viscous dissipation is neglected because of the low flow rates.

The uniform velocity field and a constant temperature are imposed at the channel inlet, while at the outlet the partial derivates of the velocity and temperature in the stream-wise direction are vanishing;

The conjugate heat transfer and no-slip velocity conditions at the solid-fluid contact are considered;

The conjugate heat transfer procedure, implies the continuity of the temperature and heat flux at a solid – liquid contact defined as,

$x = R_i$: $T_s|_{R+} = T_f|_{R-}$

$$k_S\left(\frac{\partial T_S}{\partial x}\right)_{R+} = k_f\left(\frac{\partial T_f}{\partial x}\right)_{R-}$$

$y = R_i$: $T_s|_{R+} = T_f|_{R-}$

$$k_S\left(\frac{\partial T_S}{\partial y}\right)_{R+} = k_f\left(\frac{\partial T_f}{\partial y}\right)_{R-}$$

Also at the inlet cross-section:

$$y = R_i + h_{ch};\ R_i - w_{ch} < x < R;\ 0 < z < l_{ch}/2$$

$M = M_{in}$ and $T = T_{in}$

To reduce the analysis to swirl flow phenomena, the outer surfaces of the heat sink are insulated, except the bottom one in contact with a chip:

$$y = -[H - (D_i + h_{ch}) + R_i];\ -w_m < x < w_m;\ 0 < z < L/2$$

$$q = k_S \frac{\partial T}{\partial y}$$

At the outlet of the microtube, the following boundary conditions are prescribed:

$$z = L/2$$

$$\frac{\partial v}{\partial z}=0;\frac{\partial w}{\partial z}=0;\frac{\partial u}{\partial z}=0;\frac{\partial T}{\partial z}=0$$

At the symmetry boundaries:

$z = 0$

$$\frac{\partial v}{\partial z}=0;\frac{\partial w}{\partial z}=0;\frac{\partial u}{\partial z}=0;\frac{\partial T}{\partial z}=0$$

$x = \pm w_m/2$

$$\frac{\partial v}{\partial x}=0;\frac{\partial w}{\partial x}=0;\frac{\partial u}{\partial x}=0;\frac{\partial T}{\partial x}=0$$

The partial differential equations and the boundary conditions are solved using the Fluent commercial solver [24]. The Simple algorithm is used for the velocity-pressure coupling solution and second order upwind scheme for a discretization of the equations. The under-relaxation coefficients are used for the pressure field ($\alpha = 0.3$) and momentum conservation ($\alpha = 0.7$). The convergence of the numerical solution is defined as:

$$R^{\phi}=\frac{\sum cells,P\left|\sum nb\ a_{nb}\cdot\phi_{nb}+b-a_p\phi_p\right|}{\sum cells,P\left|a_p\phi_p\right|} \quad (4)$$

The residuals for velocity components and continuity equation were 10^{-5} and for the temperature field 10^{-8}. Three different grids have been used to test the grid sensitivity, 1(414 cells at each cross-section, 200 subdivisions in the axial direction with total of 82800 cells), 2 (646,250,161500) and 3 (1020,313,319260). In Fig. (**3**), the temperature distribution at the centerline of the heat sink bottom surface is presented. The difference between the grids 2 and 3 is about 1.5 % along the axial direction, so the grid nr. 2 is used for further calculations.

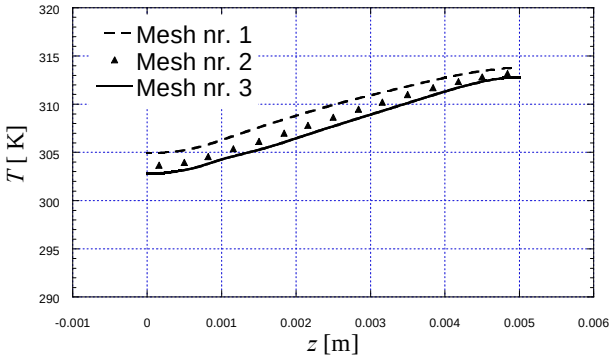

Fig. (3). Grid independence test.

RESULTS AND DISCUSSION

The results obtained for the velocity, pressure and temperature filed are used to calculate the thermal resistance and pumping power. The thermal resistance is calculated as:

$$R=\frac{T_{\max}-T_{in}}{q} \quad (5)$$

while the pumping power is defined as:

$$D = M\cdot\frac{\Delta p}{\rho} \quad (6)$$

The pressure difference is calculated as a difference between the average values at the inlet and outlet cross-sections:

$$\Delta p = p_{in} - p_{out} \quad (7)$$

Also the Re is defined as:

$$\mathrm{Re}=\frac{4\cdot(M/2)}{\pi\cdot D\cdot\mu} \quad (8)$$

In the Fig. (**4**), the temperature distribution along the centerline of a heated surface is presented for two arrangements and a higher pumping power. The jet impingement arrangement has both a lower peak temperature (T=304.84 K) and a lower temperature difference (ΔT=2.5 K) compared to the classic microtube heat sink (T=312.82 K) and (ΔT=9.8 K). In this case the temperature behavior of the jet impingement heat sink has two separate zones outside the jet impingement region. Each one has a variation similar to boundary layer behavior. This means that a swirl flow formed in the jet impingement zone is influencing the downstream portion of the microtube.

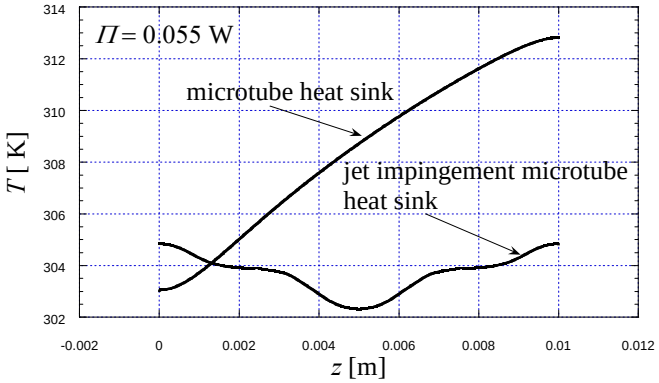

Fig. (4). The temperature distribution of a bottom heat sink surface along the fluid flow for Π = 0.055 W and for two different arrangements.

In the jet impingement region the temperature is almost constant, while in the outside region the temperature variation exhibits almost the boundary layer behavior. So for the lower pumping powers or mass flow rates, the impingement jet zone has a negligible influence on the rest of the microtube.

The same conclusion is outlined from the Fig. (**5**). The axial velocity distribution along the microtube is presented for the whole range of the mass flow rates $M = 10\cdot10^{-5}$–$10\cdot10^{-5}$ kg/s. For the lower $M = 10\cdot10^{-5}$ and $20\cdot10^{-5}$ the velocity distribution outside the jet impingement region is similar to the axial velocity variation of a classic microtube. For the

moderate $M = 20 \cdot 10^{-5}$ - $60 \cdot 10^{-5}$ the swirl flow is observed up to $L = 0.002$ m. If the mass flow rates are $M = 60 \cdot 10^{-5}$ – $90 \cdot 10^{-5}$ kg/s the flow instabilities are observed at $L = 0.003$ – 0.005 m. For the mass flow rates larger than $M = 90 \cdot 10^{-5}$ – $110 \cdot 10^{-5}$ kg/s, the axial velocity distribution has the same behavior. In this case the swirl flow is observed along the entire length of the microtube. The mass flow range $M = 60 \cdot 10^{-5}$ – $90 \cdot 10^{-5}$ kg/s corresponds to a Re = 1273 – 1910, that is still inside the laminar regime.

The flow instabilities and a thermal resistance discontinuity mentioned above, might be explained in the following manner. The flow phenomena include both the swirl flow and an axial boundary layer flow. For low and moderate mass flow rates, the swirl flow is influencing only the impingement region and a short portion of the microtube. For the mass flow rates $M = 60 \cdot 10^{-5}$ – $90 \cdot 10^{-5}$ kg/s, the swirl flow and the boundary flow have the same intensity. So the flow instabilities are produced in a zone outside the jet impingement region. For the mass flow rates greater than $M = 90 \cdot 10^{-5}$ the swirl flow prevails over the entire length of the microtube.

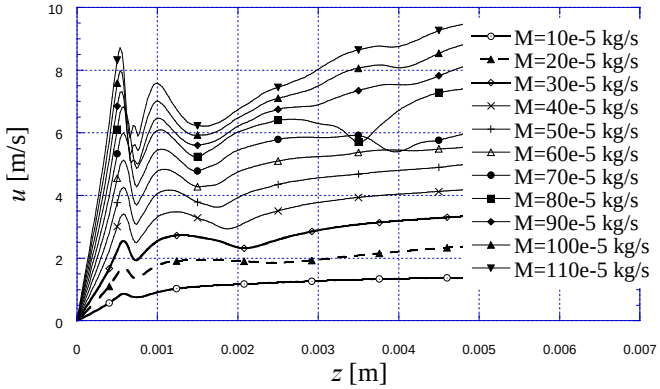

Fig. (5). The axial velocity distribution at the microtube axis for various mass flow rates and single microtube.

This conclusion can be confirmed by the axial velocity path lines presented in the Figs. (**6** and **7**) for the lower $M = 20 \cdot 10^{-5}$ and higher $M = 110 \cdot 10^{-5}$. For the lower mass flow rates, the path lines have a predominant axial direction in the zone outside the jet impingement region. Contrary, for the larger mass flow rates, the axial velocity path lines have a swirl behavior outside the inlet zone.

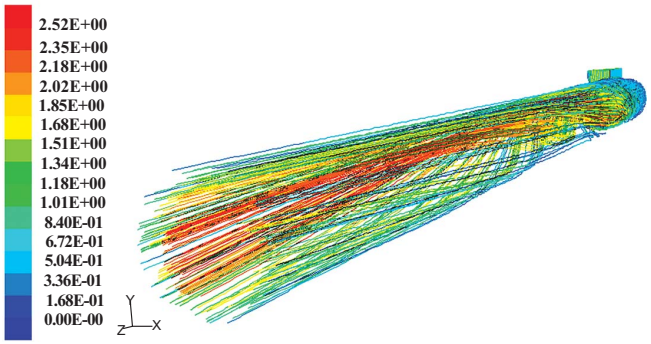

Fig. (6). The axial velocity path lines for a single microtube mass flow rate M = 20 10^{-5} kg/s.

Fig. (7). The axial velocity path lines for a single microtube mass flow rate M = 110 10^{-5} kg/s.

CONCLUSIONS

The numerical analysis of the microtube heat sink with the tangential jet impingement is presented. The obtained temperature and velocity fields are used for the performance evaluation against the classic microtube heat sink, in terms of the thermal resistance and pumping power. It is concluded that both, lower peak temperature and lower temperature difference are associated to the jet impingement heat sink.

Second, the flow instability and thermal resistance discontinuity are observed for the mass flow rates $M = 60 \cdot 10^{-5}$ – $90 \cdot 10^{-5}$ kg/s. This is explained by the fluid flow behavior of the boundary layer and swirl flow. For the lower mass flow rates, the first one is predominant while for the higher mass flow rates the second one prevails.

NOMENCLATURE

B, m,	=	width of the micro-heat sink
c_p , J/kg K,	=	specific heat
D_i, m,	=	inner diameter
h_{ch}, m,	=	channel height
H, m,	=	micro-heat sink height
k, W/m K,	=	thermal conductivity
L_{ch} , m,	=	channel length
L, m,	=	micro-heat sink length
M, kg/s,	=	mass flow rate
Δp, Pa,	=	pressure drop
q, W/cm^2,	=	heat flux
R, cm K/W,	=	thermal resistance
Re, -,	=	Reynolds number
T, K,	=	temperature
T_{max}, K,	=	peak temperature
ΔT, K,	=	temperature difference
u, v, w, m/s,	=	velocity

w_m , m, = module width

x, y, z, m, = coordinate

Greek Symbols

μ, Pa s, = dynamic viscosity

ρ, kg/m^3, = density

Π, W, = pumping power

Subscripts

in, = inlet

out, = outlet

f, = fluid

s, = solid

REFERENCES

[1] D. B. Tuckerman, R. F. W. Pease, "High-performance heat sinking for VLSI", *IEEE Electron.Device Lett.*, EDL-2 ; pp. 126-129, May 1981.

[2] W. Qu, I. Mudawar, "Experimental and numerical study of pressure drop and heat transfer in single-phase micro-channel heat sink", *Int. J. Heat Mass Trans.*, Vol. 45, pp. 2549-2565, June 2002.

[3] Fedorov, R. Viskanta, "Three dimensional conjugate heat transfer in the microchannel heat sink for electronic packaging", *Int. J. Heat Mass Trans.*, Vol. 41, pp. 399-415, Jan. 2000.

[4] M.M. Rahman, "Measurements of heat transfer in microchannels heat sinks", *Int. Comm. Heat Mass Trans.*, Vol. 27, pp. 495 - 506, May 2000.

[5] X. Yin, H.H. Bau, "Uniform channel micro heat exchangers", *ASME J. Electron. Pack.*, Vol. 119, pp. 89-94, June 1997b.

[6] H.Y.Zhang, D.Pinjala, T.N.Wong, K.C.Toh, Y.K.Joshi, "Single-phase liquid cooled microchannel heat sink for electronic packages", *App. Thermal Eng.*, Vol. 25, pp. 1472-1487, July 2005.

[7] J.Li, G.P.Peterson, P.Cheng, "Three-dimensional analysis of heat transfer in a micro-heat sink with single phase flow", *Int. J. Heat Mass Trans.*, Vol. 47, pp. 4215 - 4231, Sep. 2004.

[8] K. Vafai, L. Zhu, "Analysis of two-layered micro-channel heat sink concept in electronic cooling", *Int. J. Heat Mass Trans.*, Vol. 42, pp. 2287-2297, June 1999.

[9] X. Wei, Y.K. Joshi, "Stacked microchannel heat sinks for liquid cooling of microelectronics component", *ASME J. Electron. Pack.*, Vol. 126, pp. 60-66, March 2004.

[10] M.K. Patterson, X. Wei, Y. Joshi, R. Prasher, "Numerical study of conjugate heat transfer in stacked microchannel", Inter Society Conference on Thermal Phenomena, 2004, pp. 372-380.

[11] S.J. Kim, D. Kim, "Forced convection in microstructures for electronic equipment cooling", *ASME J. Heat Trans.*, Vol. 121, pp. 639-645, Aug. 1999.

[12] S.J. Kim, D. Kim, D.Y. Lee, "On the local thermal equilibrium in microchannel heat sink", *Int. J. Heat Mass Trans.*, Vol. 43, pp. 1735 - 1748, May 2000.

[13] R.W. Knight, D.J. Hall, J.S. Goodling, R.C. Jaeger, "Heat sink optimization with application to microchannels", *IEEE Trans. Comp. Hyb. Manufact. Tech.*, Vol. 15, pp. 832-842, June 1992.

[14] S.H., Chong, K.T. Ooi, T.N. Wong, "Optimization of single and double layer counter flow microchannel heat sinks", *App. Thermal Eng.*, Vol. 22, pp. 1569-1585, Oct. 2002.

[15] Hassan, Thermal-Fluid Mems devices, "A decade of progress and challenges ahead", *ASME J. Heat Trans.*, Vol. 128, pp. 1221-1233, Nov. 2006.

[16] S.V. Garimella, C.B. Sobhan, "Transport in microchannels - a critical review", *Ann. Rev. Heat Trans.*, Vol. 13, pp. 1-50, Jan. 2003.

[17] C.J. Kroeker, H.M. Soliman, S.J. Ormiston, "Three-dimensional thermal analysis of heat sinks with circular cooling microchannels", *Int. J. Heat Mass Trans.*, Vol. 47, pp. 4733 - 4744, Oct. 2004.

[18] J.H. Ryu, D.H. Choi, S.J. Kim, "Three-dimensional numerical optimization of a manifold microchannel heat sink", *Int. J. Heat Mass Trans.*, Vol. 46, pp. 1553-1562, April 2003.

[19] M.K. Sung, I. Mudawar, "Experimental and numerical investigation of single-phase heat transfer using a hybrid jet-impingement/micro-channel cooling scheme", *Int. J. Heat Mass Trans.*, Vol. 49, pp. 682 - 694, Feb. 2006.

[20] T. Bello-Ochende, L. Liebenberg, J.P. Meyer, "Constructal cooling channels for micro-channel heat sinks", *Int. J. Heat Mass Trans.*, Vol. 50, pp. 4141 - 4150, Oct. 2007.

[21] T. Bello-Ochende, L. Liebenberg, J.P. Meyer, A.G. Malan, A. Bejan, "Constructal conjugate heat transfer in three dimensional cooling channels", *J. Enh. Heat Trans.*, Vol. 14, pp. 279 -293, Oct. 2007.

[22] D. Lelea, S. Nishio, K. Takano, "The experimental research on microtube heat transfer and fluid flow of distilled water", *Int. J. Heat Mass Trans.*, Vol. 47, pp. 2817-2830, June 2004.

[23] D. Lelea, "Some considerations on frictional losses evaluation of a water flow in microtubes", *Int. Comm. Heat Mass Trans.*, Vol. 32, pp. 964-973, July 2005.

[24] Fluent 6.1.22 documentation, Fluent Inc. 2003.

Received: March 31, 2008 Revised: April 30, 2008 Accepted: April 30, 2008